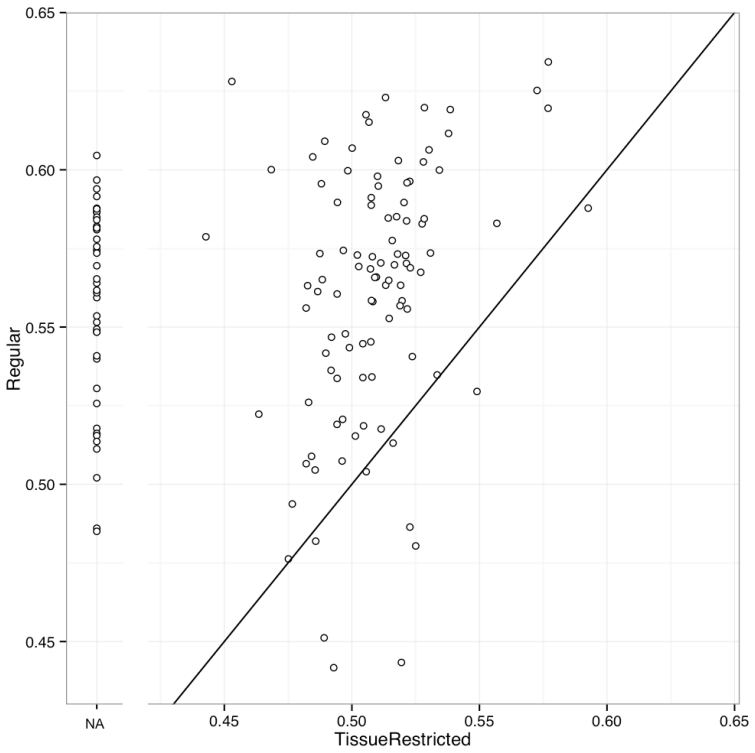

Supplementary Figure 1: Integrating the entire data compendium with hierarchy-aware tissue-specific knowledge generates networks that better capture tissue-specific interactions than limiting the integration to tissue-specific data (p = 1.3e-9). For each tissue, two networks – one integrating the entire data compendium, and other integrating only tissue labeled data – were generated, and their performance was measured using area under the receiver operator curve (AUC) based on cross-validation. The scatterplot shows that the performance for 64 tissues (points) with tissue-labeled data (x-axis) and all data (y-axis), with 62 of 64 performing better with all data (above the diagonal line; p = 3.2e-12). The remaining 80 tissues did not have sufficient tissue-specific data (fewer than 5 datasets) available to perform a tissue-restricted integration. The performance of our Bayesian integration for these tissues is shown on the disconnected axis.

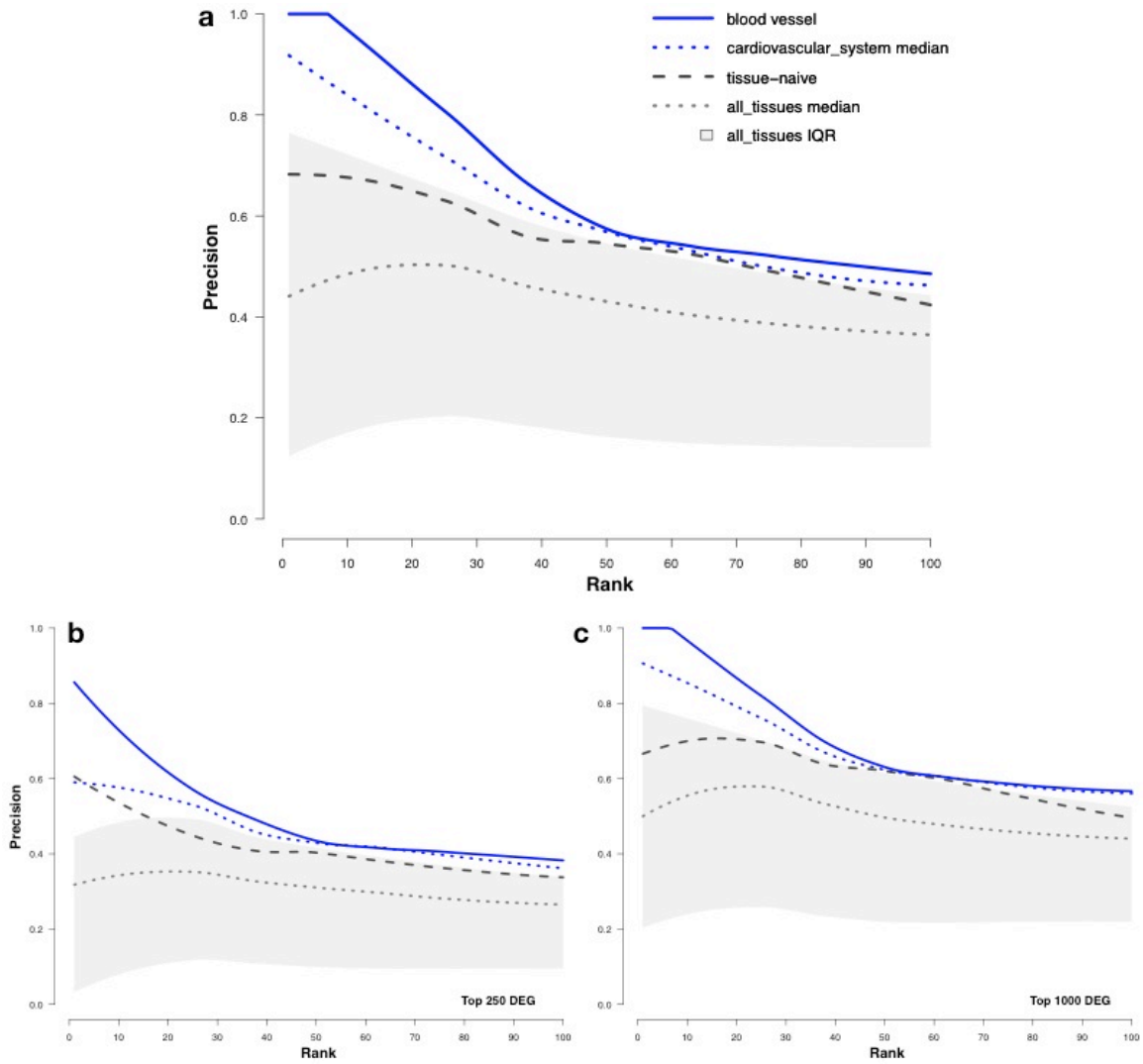

Supplementary Figure 2: The *blood vessel* and *cardiovascular system* networks show the best correspondence with the experiment, over and above the tissue-naïve network and the bulk of other unrelated tissue networks. For each network, genes were ranked based on their connectivity to IL-1β in that network. Then, at each rank, the precision of the predictions up to that rank was calculated as the fraction of genes that are differentially expressed in the experiment. Plotted in each of the three graphs is the precision (y-axis) at incremental sets of top-ranked genes (1-100; x-axis). The precision for the *blood vessel* and tissue-naïve networks are plotted in solid blue and dashed dark-grey, respectively. The median precision at each rank for the cardiovascular system of tissues, and all tissues are plotted in dotted blue and grey, respectively. Further, the grey band around the *all_tissues* median represents the inter-quartile range of precision values at each rank calculated across all tissues. The three plots correspond to different choices of differentially expressed genes (DEG) from the microarray, with (A) 500 genes, (B) 250 genes, and (C) 1000 genes. The results in the main text are based on choosing genes from (A) at rank 20.

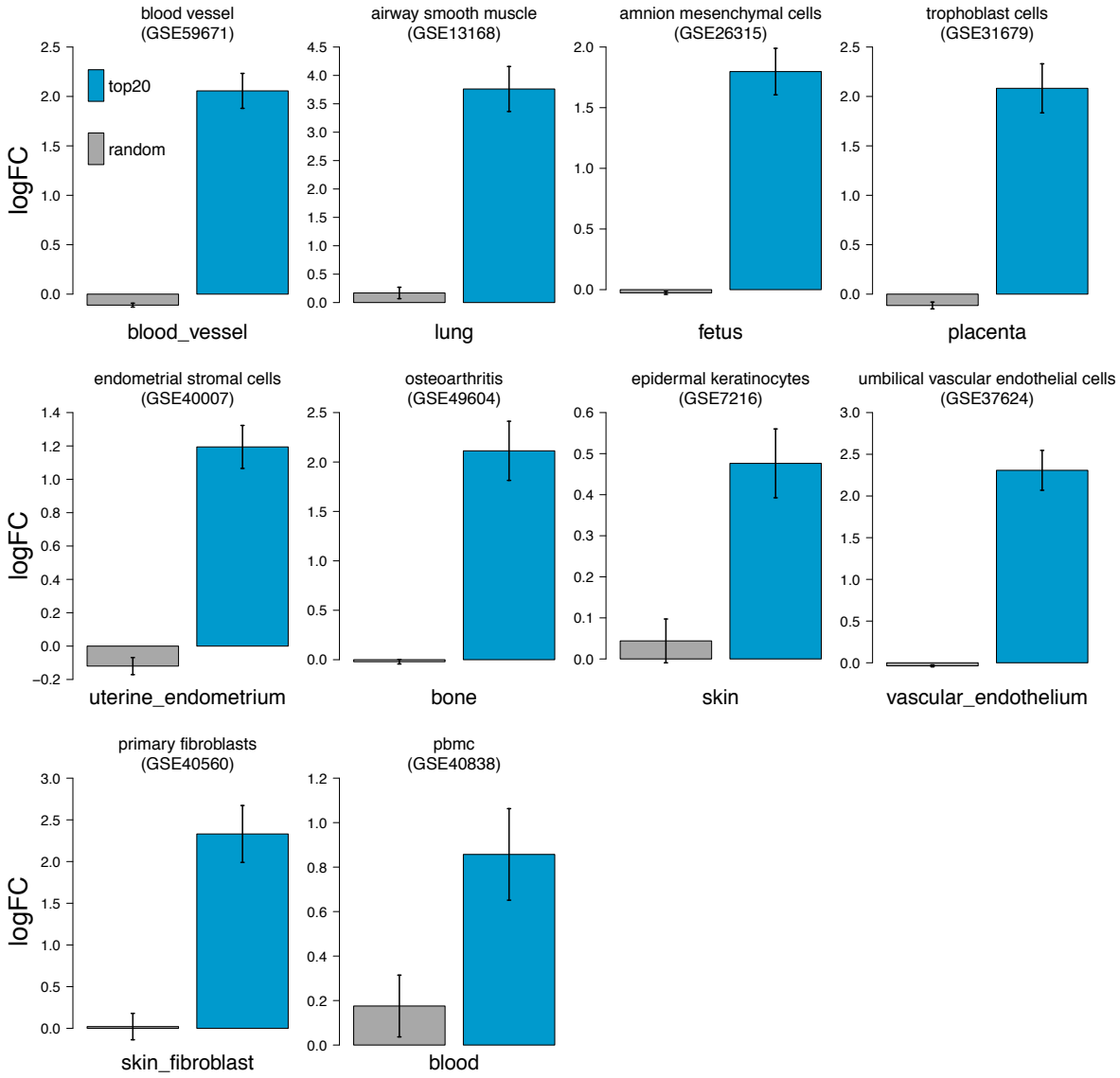

Supplementary Figure 3: We analyzed publicly available gene expression datasets that included IL-1β treatment and found that genes connected to IL-1β in tissue-specific networks for the corresponding tissue responded significantly to treatment. Each plot shows the mean $\log_2$ fold change after IL-1β treatment of the twenty genes most tightly connected to IL-1β in the network listed on the x-axis, and error bars represent the standard error (s.e.). Also plotted alongside as controls are the mean and s.e. of twenty random genes from the dataset. The first plot (GSE59671) corresponds to the blood vessel experiment elaborated in the main text (Fig. 2). The cell type and GEO identifier of the other datasets from which gene expression data were extracted is listed above the plot. Of these datasets, only GSE7216 (epidermal keratinocytes) is included in the data compendium used for integration. The rest are independent of the integration.

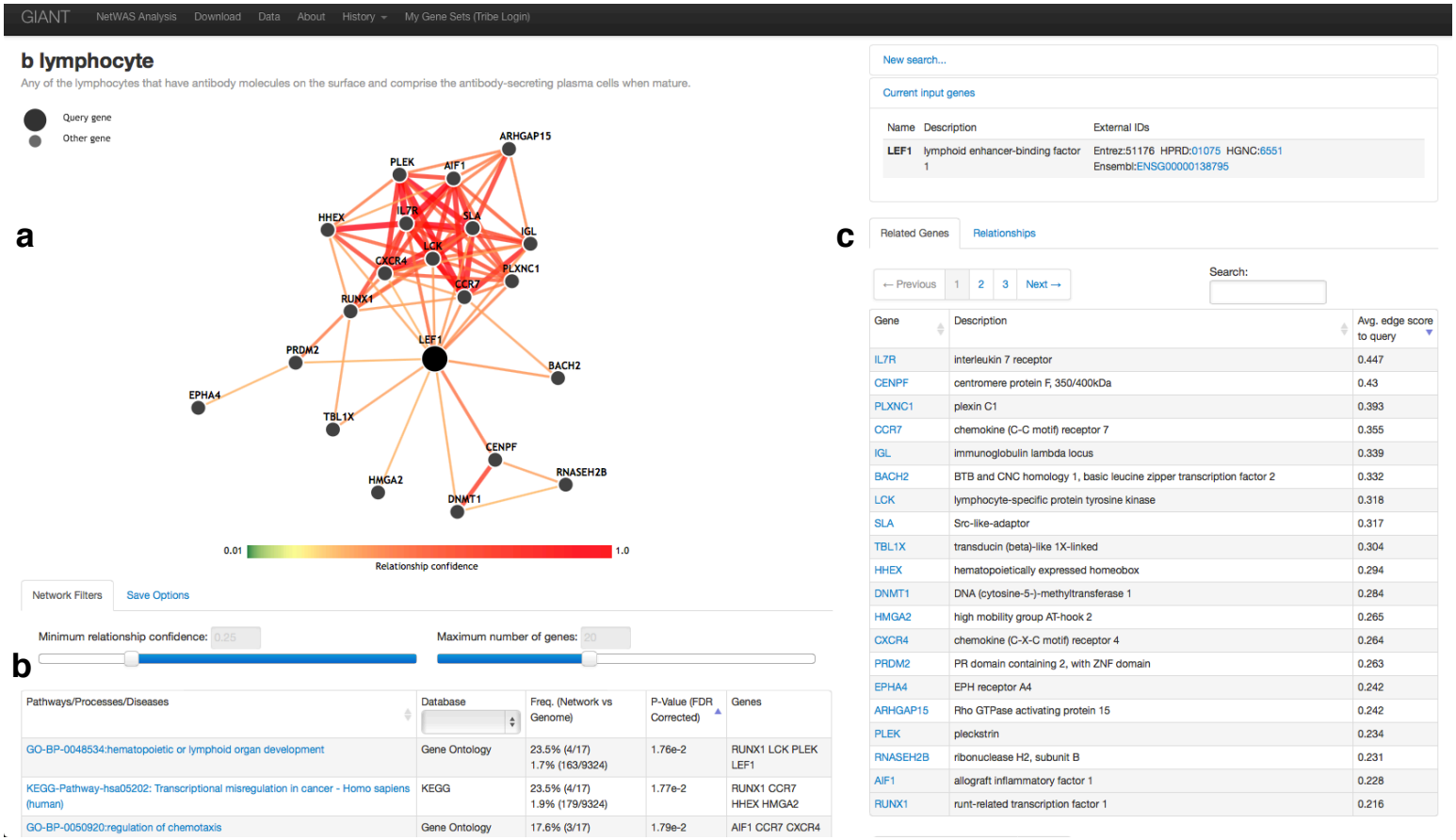

Supplementary Figure 4: Single-tissue query interface in GIANT shows LEF-1's (A) functional network neighborhood in *B-lymphocyte*, (B) functional enrichment in this neighborhood, and (C) most connected genes.

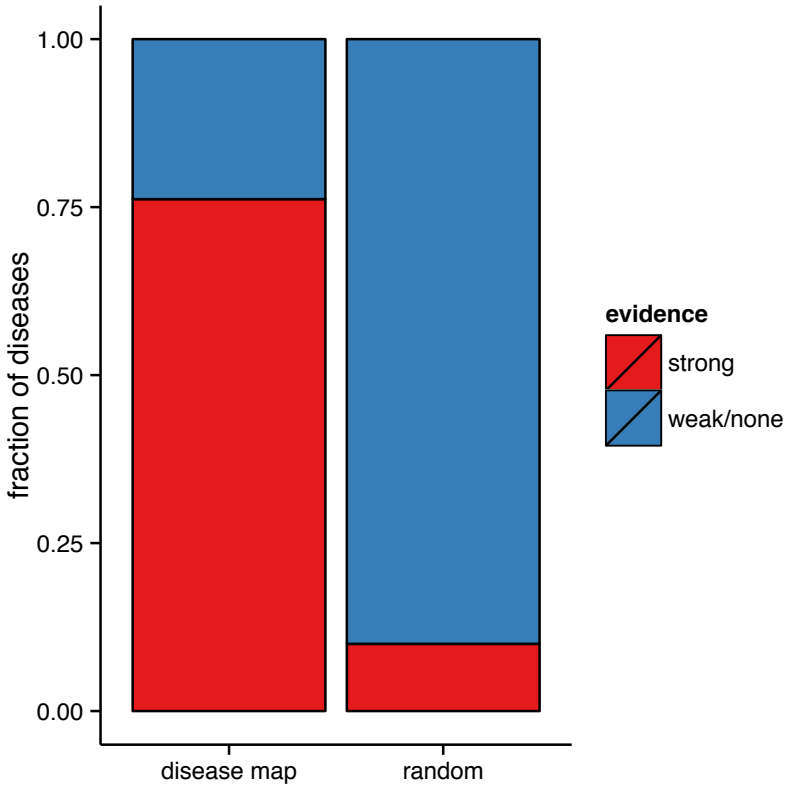

Supplementary Figure 5: This stacked bar plot shows the results of our blinded literature evaluation. Only 10% of randomly selected diseases were associated strongly to Parkinson's disease in the literature, while more than 75% of disease-map selected diseases were associated.

Supplementary Figure 6: Additional disease maps for (a) Alzheimer's disease in the temporal lobe network (z-score ≥ 2.25), (b) glycogen metabolism disorder in liver (z-score ≥ 1.75), and (c) glomerulonephritis in renal glomerulus (z-score ≥ 1.5). The appropriate tissue network was chosen based on connectivity of diseases in their relevant tissues (see '*Network connectivity in tissue-specific processes*' in *Methods*).

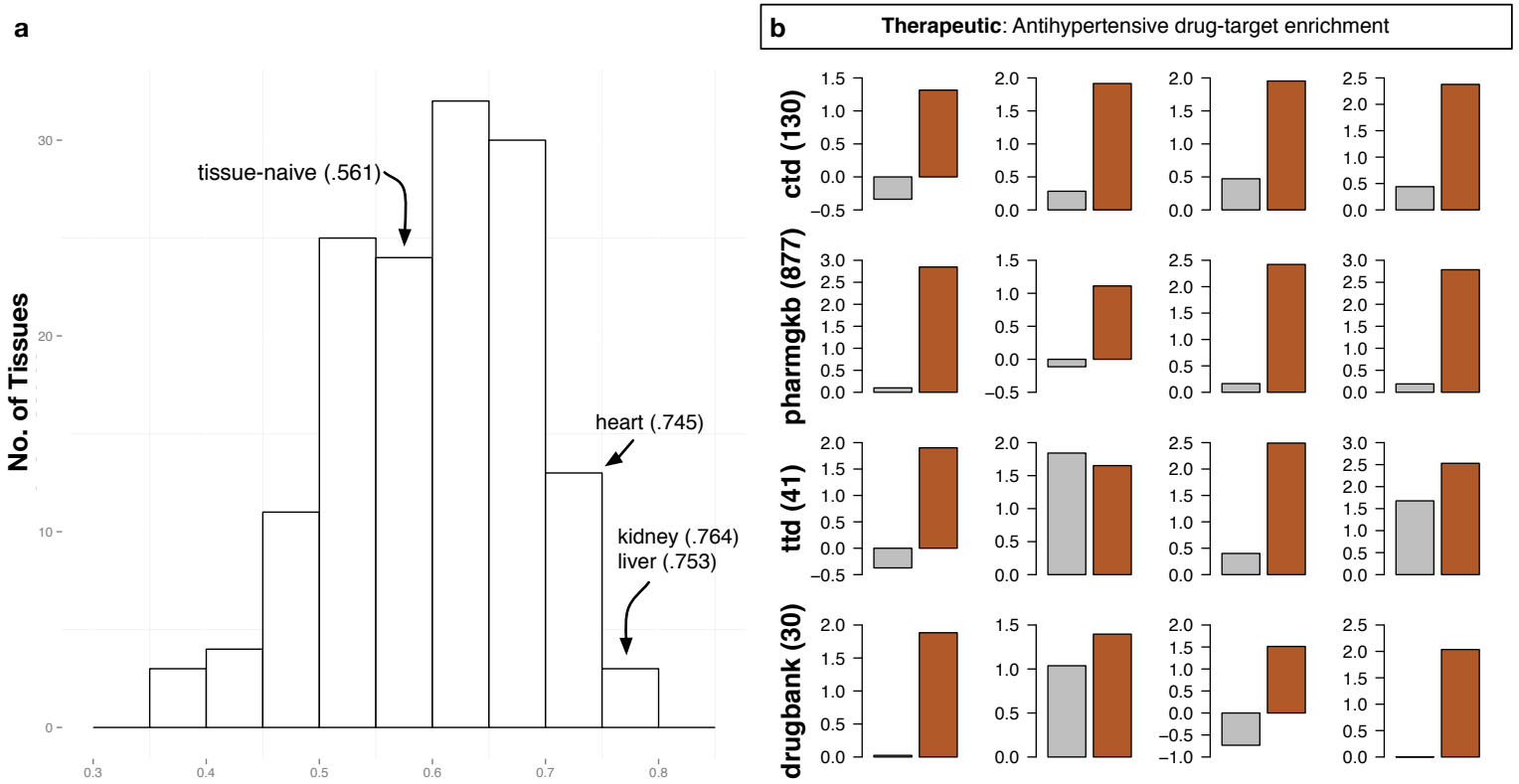

Supplementary Figure 7. (A) Relevant tissue networks show the best performance in reprioritizing hypertension GWAS. In order to evaluate the choice of tissues for reprioritization, we evaluated all tissue networks (along with the tissue-naïve network) in the same setting as we used for the *kidney* network. The distribution of performance (measured using AUC) shows that the right tissue network, *kidney*, and other relevant tissues, *heart* and *liver,* are among the best, while the tissue-naïve network sits amidst tissue networks that provide an average performance. (B) Top-ranked genes by NetWAS are significantly enriched with targets of antihypertensive drugs. Drug-targets were obtained from four databases – DrugBank, TTD, PharmGKB, and CTD – which curate this information using different criteria. We evaluated both the original GWAS (grey) and NetWAS using the *kidney* network (dark red) for enrichment of drug-targets from each of these sources among the top-ranked genes. Enrichment was measures using z-scores (see Methods), with higher scores indicating greater enrichment near the top of the list. In nearly all cases – target data sources and phenotypic end-points – NetWAS reprioritization resulted in a significant top-ranking of therapeutic targets, over the original GWAS.

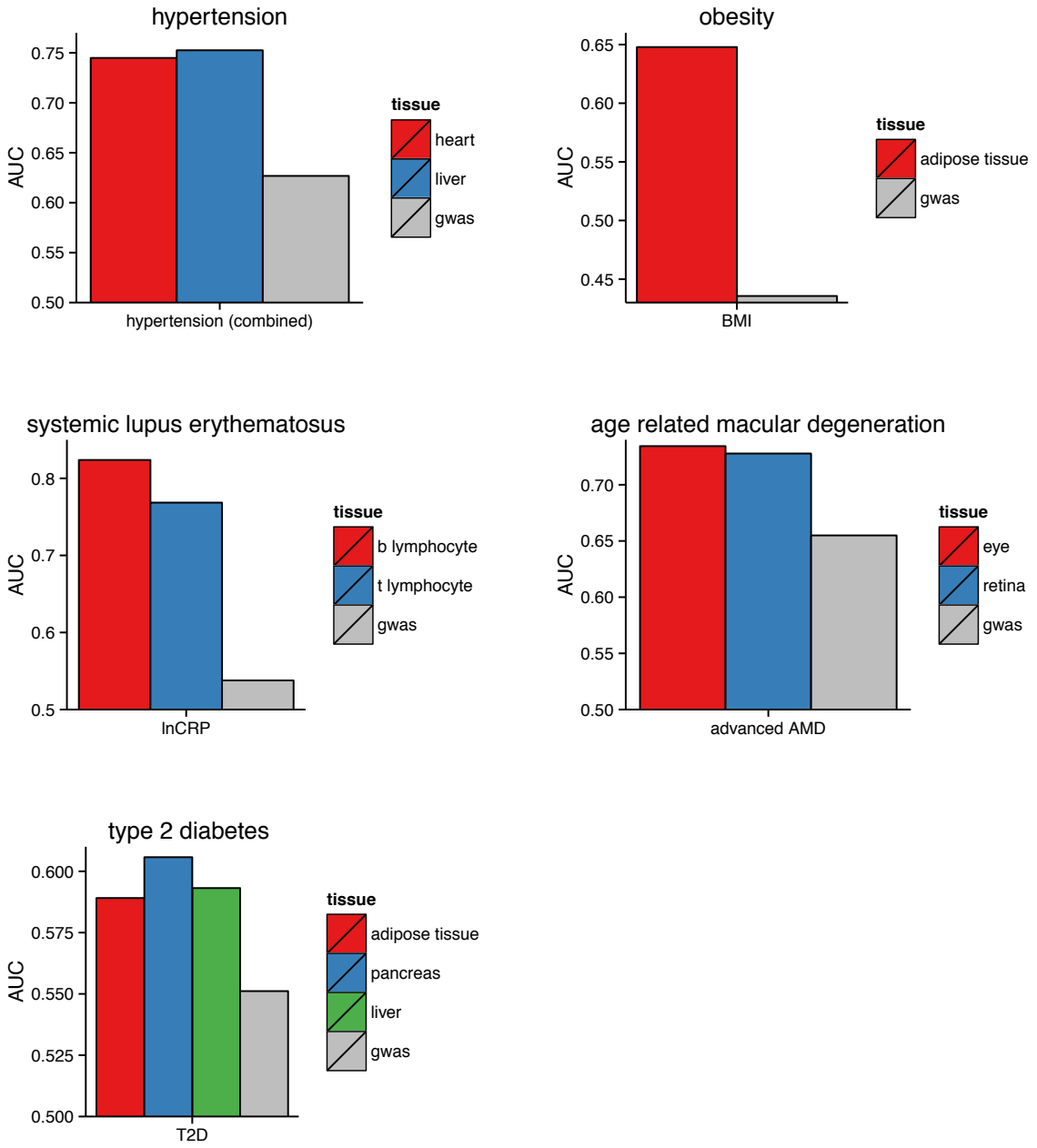

Supplementary Figure 8: NetWAS reprioritization is effective across studies, phenotypes, and relevant networks. Each bar shows the performance of NetWAS reprioritization as measured by the area under the curve (AUC) of documented disease associations with the disease specified in the label above the plot. The horizontal axis shows relevant networks (colored bars) and GWAS alone (grey bars), and the horizontal axis label describes the GWAS phenotype from which associations were obtained.